

Electronic Supplementary Information

Direct Conversion of CO₂ to Solid Carbon by Ga-Based Liquid Metals

Karma Zuraiqi^a, Ali Zavabeti^{a,b}, Jonathan Clarke-Hannaford^c, Billy James Murdoch^c, Kalpit Shah^a, Michelle J.S. Spencer^c, Chris F. McConville^d, Torben Daeneke^{a,*}, Ken Chiang^{a,*}

^a School of Engineering, RMIT University, Melbourne, VIC 3000, Australia

^b Department of Chemical Engineering, The University of Melbourne, Parkville, Melbourne, VIC 3010, Australia

^c School of Science, RMIT University, GPO Box 2476, Melbourne, VIC 3001, Australia

^d Institute for Frontier Materials, Deakin University, Geelong, Melbourne, VIC 3220, Australia

* Correspondence: Ken.Chiang@rmit.edu.au, Torben.Daeneke@rmit.edu.au

Materials

Gallium (Ga) and Indium (In) were supplied by Roto Metals with cited purities of 99.99%. All supplied chemicals were used as received.

Methods

Alloy Synthesis

The EGaIn alloy was prepared by combining stoichiometric quantities of Ga and In (75 wt.% Ga and 25 wt.% In). The composing metals were mixed on a hot plate at about 200°C (above the melting point of In), until the metals were completely dissolved and appeared well mixed. The alloy is then allowed to cool down naturally.

CO₂ Decomposition in a Bubbling Column Reactor

Since LMs are corrosive to other metals, the bubbling column reactor (30 cm in length, 1.0 cm internal diameter) was constructed from quartz to withstand activity tests at high operating temperatures, to give high visibility, and to provide resistance to LM corrosion. Gas flow into the column was regulated with mass flow controllers (Bronkhorst EL-FLOW) and checked with non-returning valves to prevent backflow of the reactants. To analyze the gaseous products, continuous gas chromatographic measurements were carried out using a PerkinElmer Clarus 580 online GC. Heating was supplied by an external split furnace equipped with a k-type thermocouple and connected to a temperature controller. The reactor and its content were allowed to cool naturally after the reaction, and the carbon product was collected from the top of the LM melt for characterization.

Gallium expands at temperature below its melting point (when it solidifies), similar to water ice. This property of Ga therefore presents challenges when the process is operated near room temperature and will cause equipment damage if the temperature is unintentionally dropped below 30°C. These implications can be overcome by adding indium or tin to make gallium-based eutectic alloys that are liquid at room temperature.

Electrochemical Regeneration/Reduction of Gallium

The electroreduction of gallium oxide was carried out on glassy carbon, with an exposed area of 0.28 cm². Linear sweep voltammetry measurements were performed using a CHI680 Amp Booster. Potentials were measured in an aqueous solution comprised of 1M H₂SO₄, against Ag/AgCl as a reference electrode, and with platinum wire as the counter electrode.

Characterization Techniques

In-situ XPS analysis was performed on the EGaIn surface using a Kratos Axis Supra XPS spectrometer, equipped with a monochromated Al X-ray source ($h\nu = 1486.6$ eV) and a concentric hemispherical electron analyzer. Over the course of the analysis, the ambient pressure was maintained in the analysis and reaction chambers below 1.0×10^{-8} and 5.0×10^{-7} mbar respectively, and the scans were recorded using a 40 eV pass energy.

The Raman spectra of the produced carbon were acquired using a Horiba LabRam HR Evolution, equipped with a 532 nm laser. The relative intensity ratio (I_D/I_G) is calculated based on the measured intensity of the D band (originating at 1325 cm⁻¹) and the G band (originating at 1600 cm⁻¹), as obtained from the Raman spectra.

Scanning Electron Microscope (SEM) images and energy dispersive X-ray (EDX) elemental mappings were collected using an FEI Verios 460L equipped with Oxford XMax30 EDS Detector. The images and maps are collected using Elstar in-lens secondary electron detector (TLD-SE) and accelerating voltage of 30 kV, respectively.

Density Functional Theory Calculations

All calculations were performed using density functional theory (DFT) as implemented in the Vienna *ab initio* simulation package (VASP),¹⁻⁴ with the Perdew-Burke-Ernzerhof (PBE) exchange-correlation functional⁵ and the projector augmented wave (PAW) method.⁶ The Ga(4s4p) valence electrons were treated explicitly, with a previous study indicating the semi-core 3d-states to have negligible effects.⁷ A kinetic energy cut-off value of 450 eV was used to expand the wavefunctions. The DFT-D3 functional⁸ was used to account for van der Waals forces.

To model the Ga-In slab, the bulk α -Ga was first constructed, which has an orthorhombic structure with Cmca symmetry and consists of eight atoms per unit cell. The calculated lattice parameters were determined to be $4.54 \times 7.71 \times 4.56$ Å. A Monkhorst-Pack (MP) k-point mesh of $19 \times 19 \times 19$ was used to sample the Brillouin zone for the bulk α -Ga. A $2 \times 1 \times 2$ supercell was then generated from the bulk structure to represent the ‘liquid’ slab of Ga, cleaving a (010) surface from the bulk and including a 15 Å vacuum spacer to avoid interactions between the periodic images (Fig. S7).

Four Ga atoms (one for each of the four layers) were then substituted with In atoms, and *ab initio* molecular dynamics (AIMD) simulations were performed using a time step of 1 fs at 310

K until the structure had equilibrated (after ~5 to 10 ps). This was performed on three different In-doped Ga structures (Fig. 1b–d), with the initial placement of the In atoms being different in each structure. The final Ga-In structures were then used to investigate the adsorption behaviour of CO₂. For the optimization calculations and AIMD simulations, an 11 × 11 × 1 and 8 × 8 × 1 MP k-grid were used, respectively. A fermi-level smearing method was adopted, with a smearing width of 0.1 eV used for all calculations. All atoms were allowed to relax during the optimization and AIMD simulations so that the Hellmann-Feynman forces were less than 0.01 eV/Å and the total energy was converged to 10⁻⁶ eV. The binding energy (E_b) for the adsorption of CO₂ on the Ga or In-doped Ga slabs was calculated using the following expression:

$$E_b = E_{CO_2 + slab} - (E_{slab} + E_{CO_2})$$

where the total energy of the system with the adsorbed CO₂ is $E_{CO_2 + slab}$, the substrate by itself is E_{slab} and the CO₂ molecule is E_{CO_2} .

Supplementary Figures

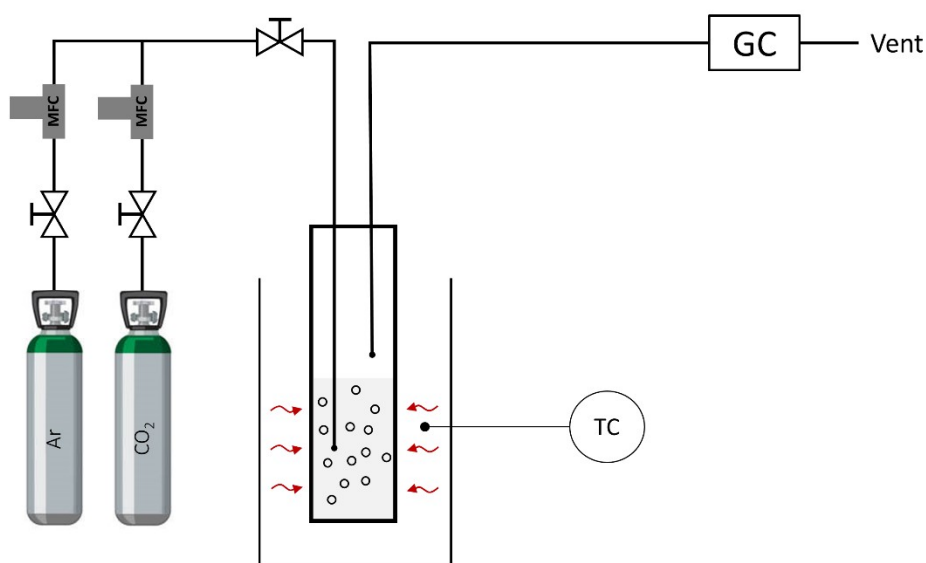


Fig. S1. Schematic of the experimental set up for the liquid metal bubbling column reactor. Volumetric flow of Ar and CO₂ entering the reactor is regulated with mass flow controllers (MFCs), and reactor temperature is regulated using a temperature controller (TC) connected to a thermocouple. Reactor effluent is periodically monitored using a fully automated gas chromatograph (GC).

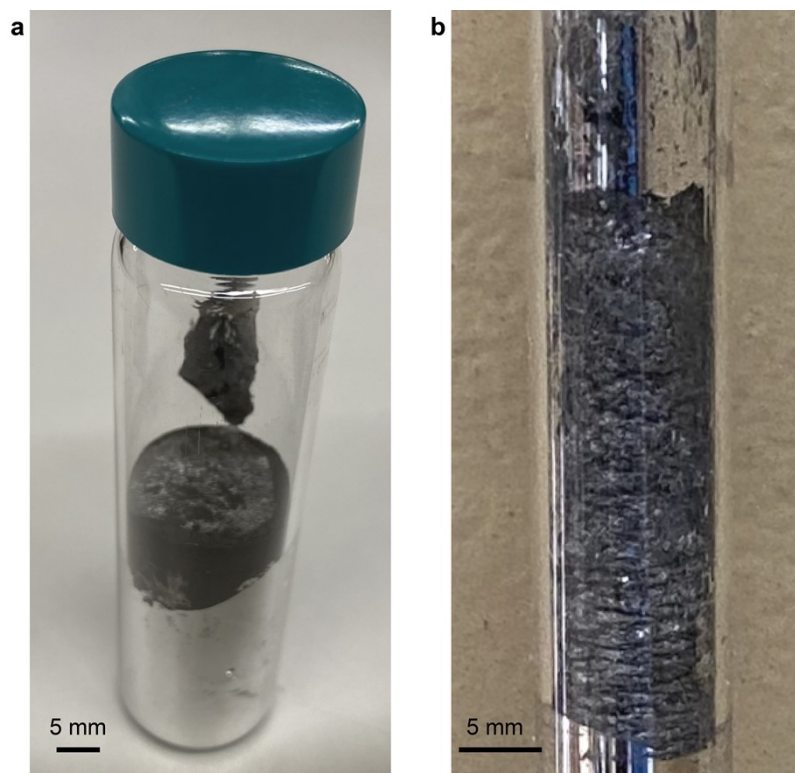


Fig. S2. An image of the carbon product accumulated above the liquid metal melt after CO₂ decomposition at (a) 200°C after 4 hours and (b) room temperature after 24 hours.

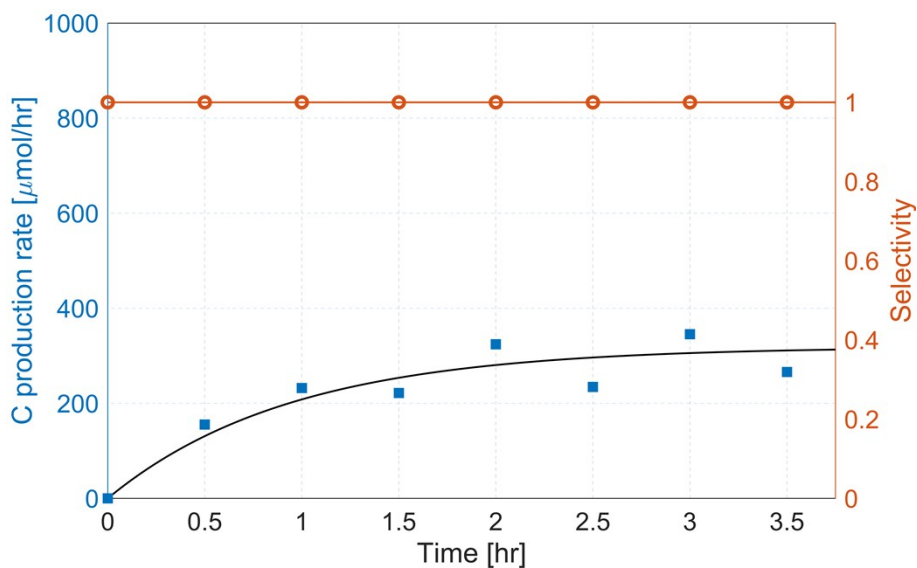


Fig. S3. Carbon production rate and carbon selectivity, under continuous flow of CO_2 over Ga in a bubbling column reactor, at 200°C and ambient pressure.

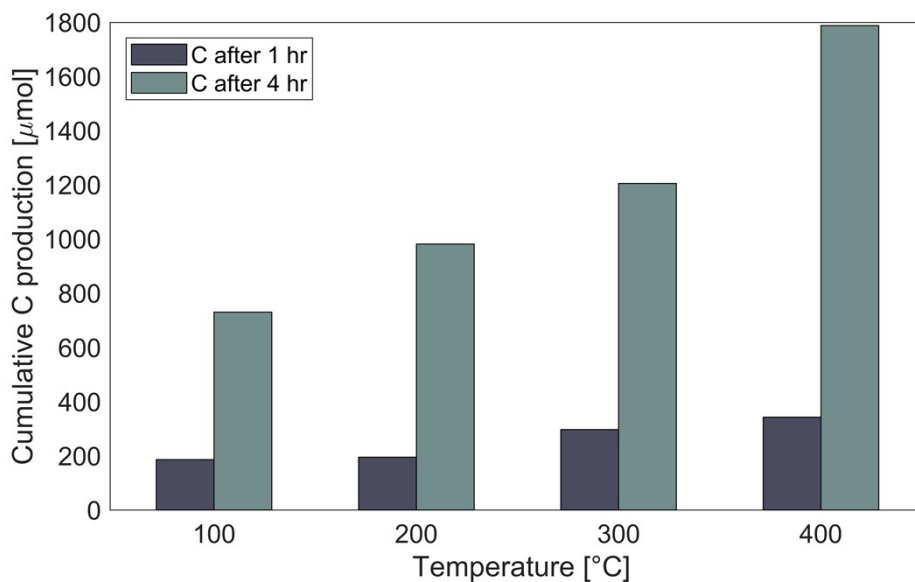


Fig. S4. Cumulative carbon production at different temperatures, showcasing the increase in the amount of carbon accumulated under continuous flow of CO_2 over EGaIn at different temperatures.

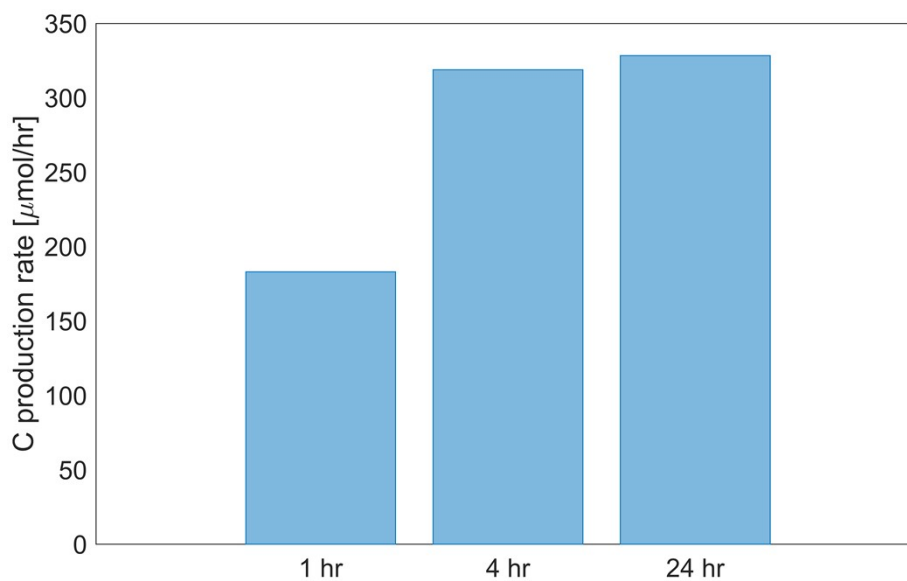


Fig. S5. Carbon production rate under continuous flow of CO_2 in a bubbling column reactor at 200°C sampled at different time snaps.

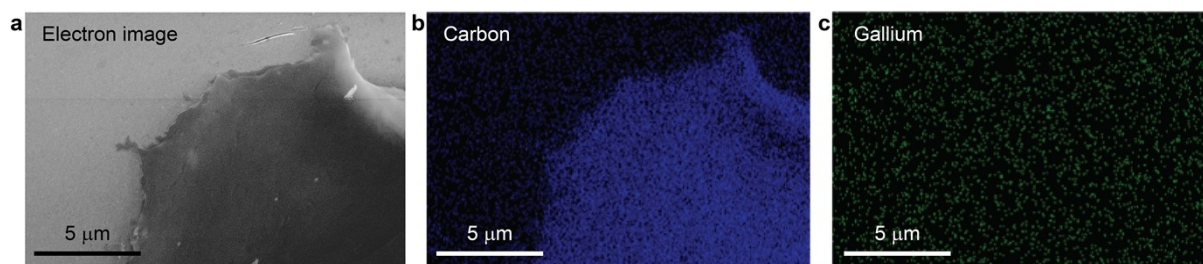


Fig. S6. SEM of the collected carbon product after CO_2 decomposition at room temperature (a) micrograph showing carbon sheets, (b) EDX elemental map showing carbon dispersion and (c) EDX elemental map showing gallium dispersion.

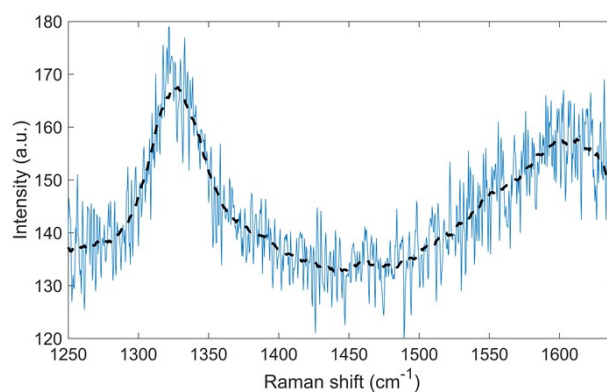


Fig. S7. Raman spectroscopy of carbon produced at room temperature, showing the characteristic D and G bands.

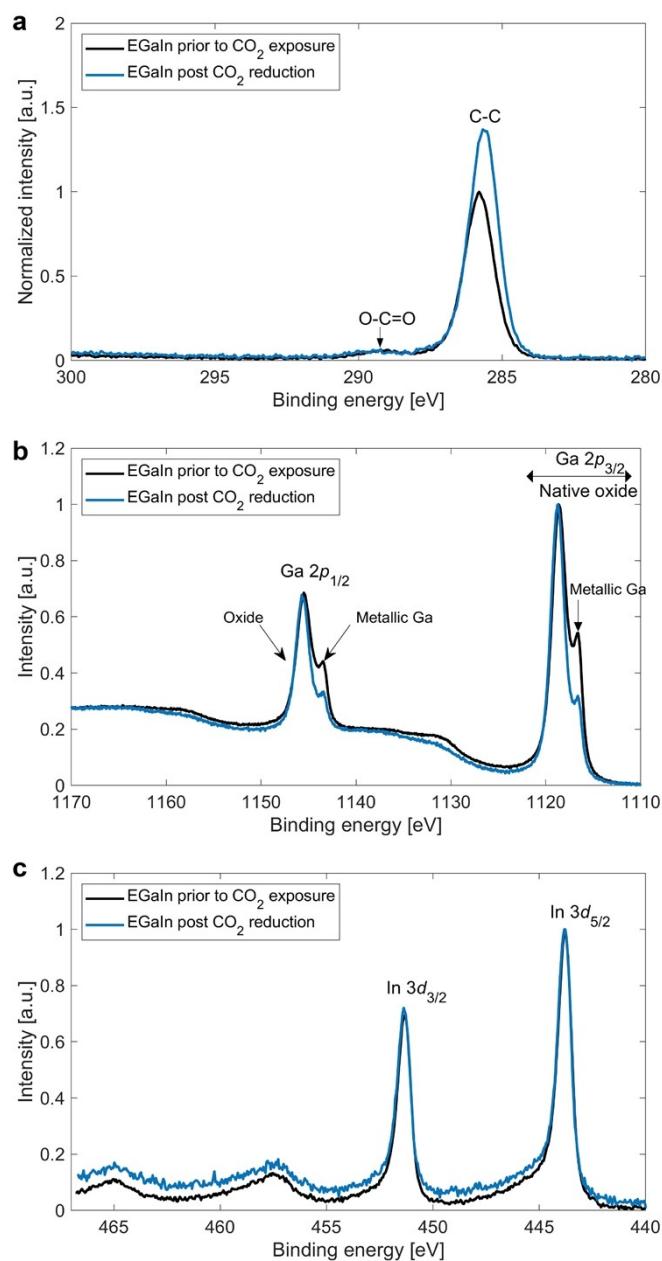


Fig. S8. In-situ XPS spectra of (a) C1s, (b) Ga 2p, and (c) In 3d regions of the thermal reduction of CO_2 at 200°C . The C1s region intensity is normalized to the Ga 2p_{3/2} peak to depict the relative increase in the (C - C) carbon content. The black line corresponds to the spectra prior to CO_2 exposure and the blue line corresponds to the spectra post CO_2 reduction.

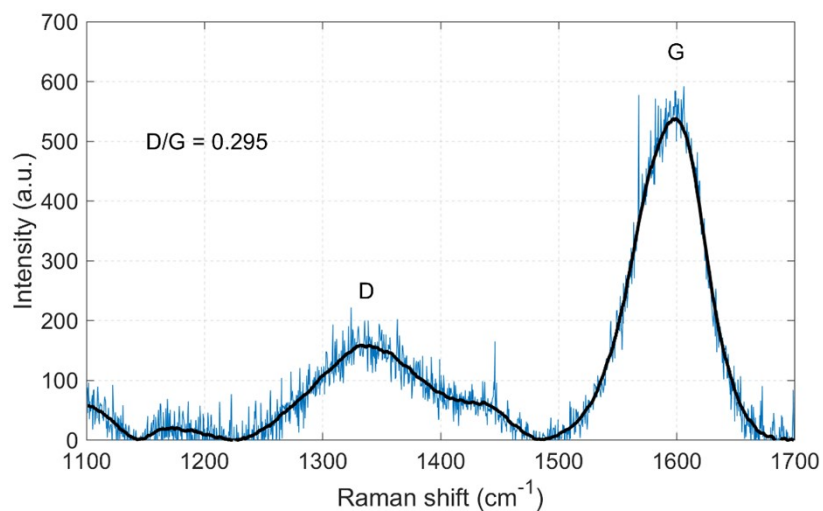


Fig. S9. Raman spectrum of the carbon product with an I_D/I_G ratio of 0.295.

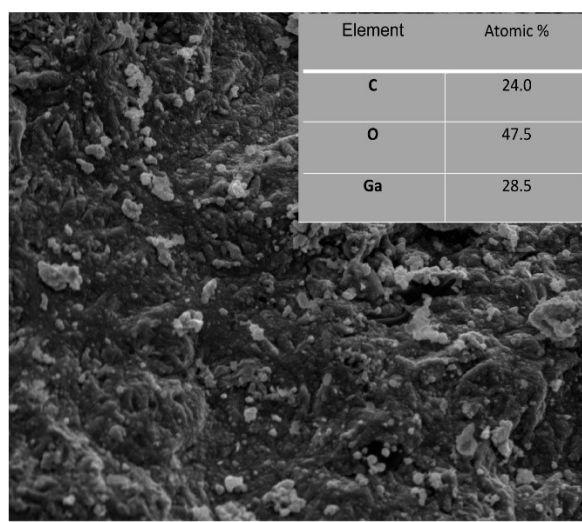


Fig. S10. SEM image of the bulk reaction product generated at 200°C, after 4 hours of continuous CO_2 decomposition. EDX analysis (inset) was conducted as a wide area scan of the complete area encompassed in the image, showing stoichiometric ratios of carbon, oxygen, and gallium.

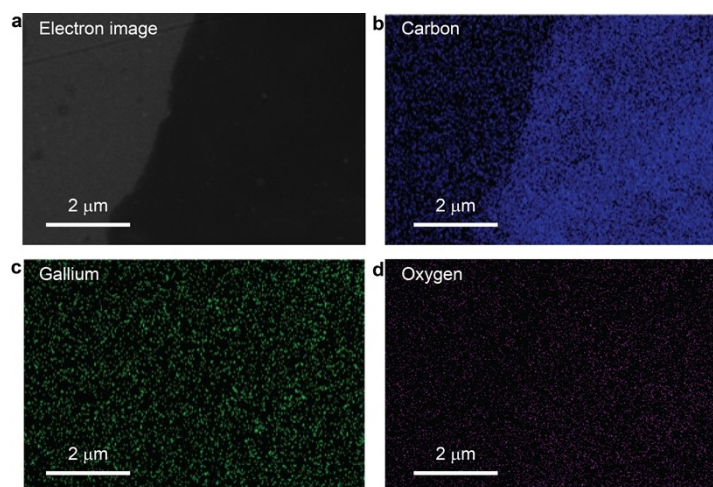


Fig. S11. SEM of the collected carbon product after CO_2 decomposition at 200°C (a) micrograph showing carbon sheets, (b) EDX elemental map showing carbon dispersion and (c) EDX elemental map showing gallium dispersion.

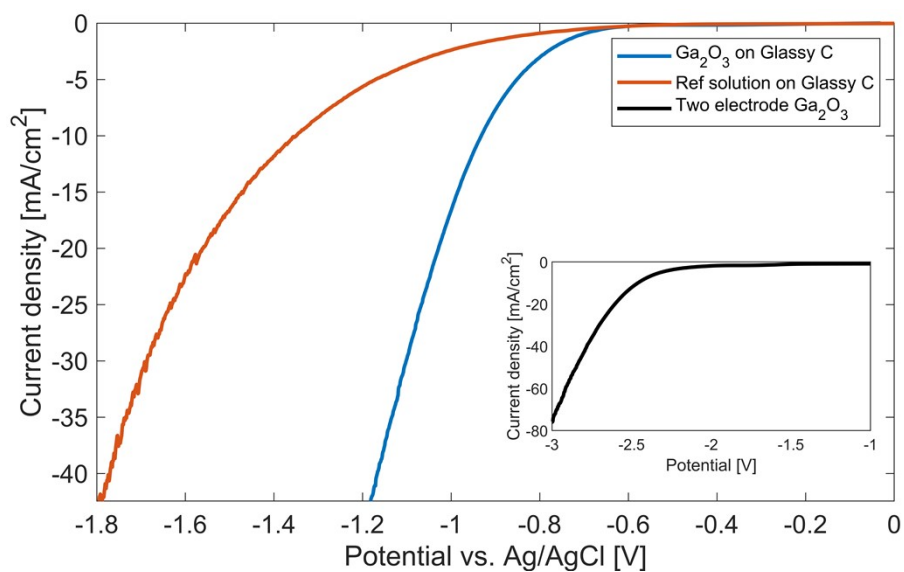


Fig. S12. Linear sweep voltammetry of gallium oxide measured in 1M H_2SO_4 compared against gallium oxide-free H_2SO_4 reference solution. Inset illustrates the onset potential of gallium oxide in a two-electrode system.

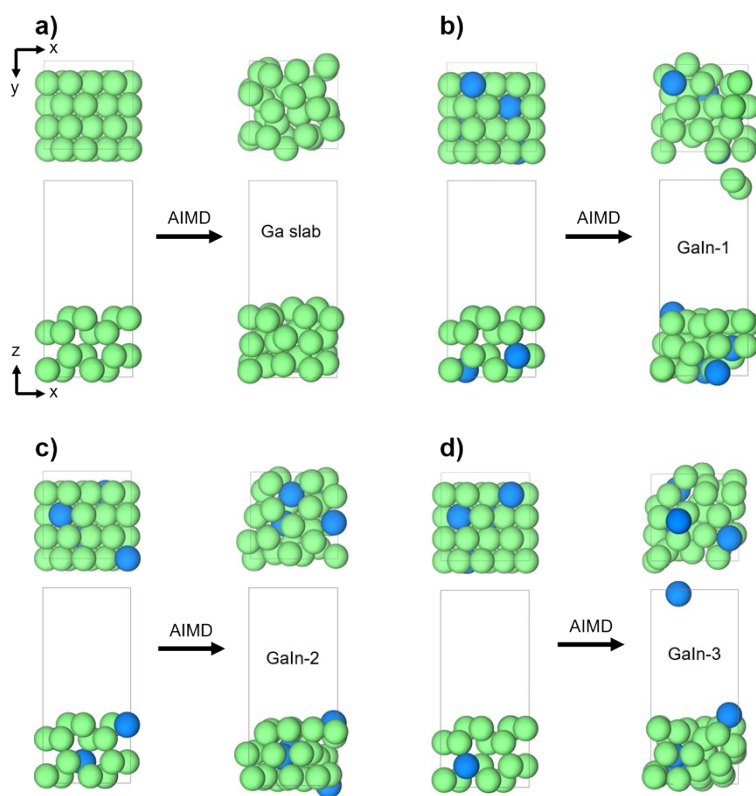


Fig. S13. The (a) clean Ga slab and (b-d) In-doped Ga slabs (GaIn) obtained after 5–10 ps of AIMD simulation.

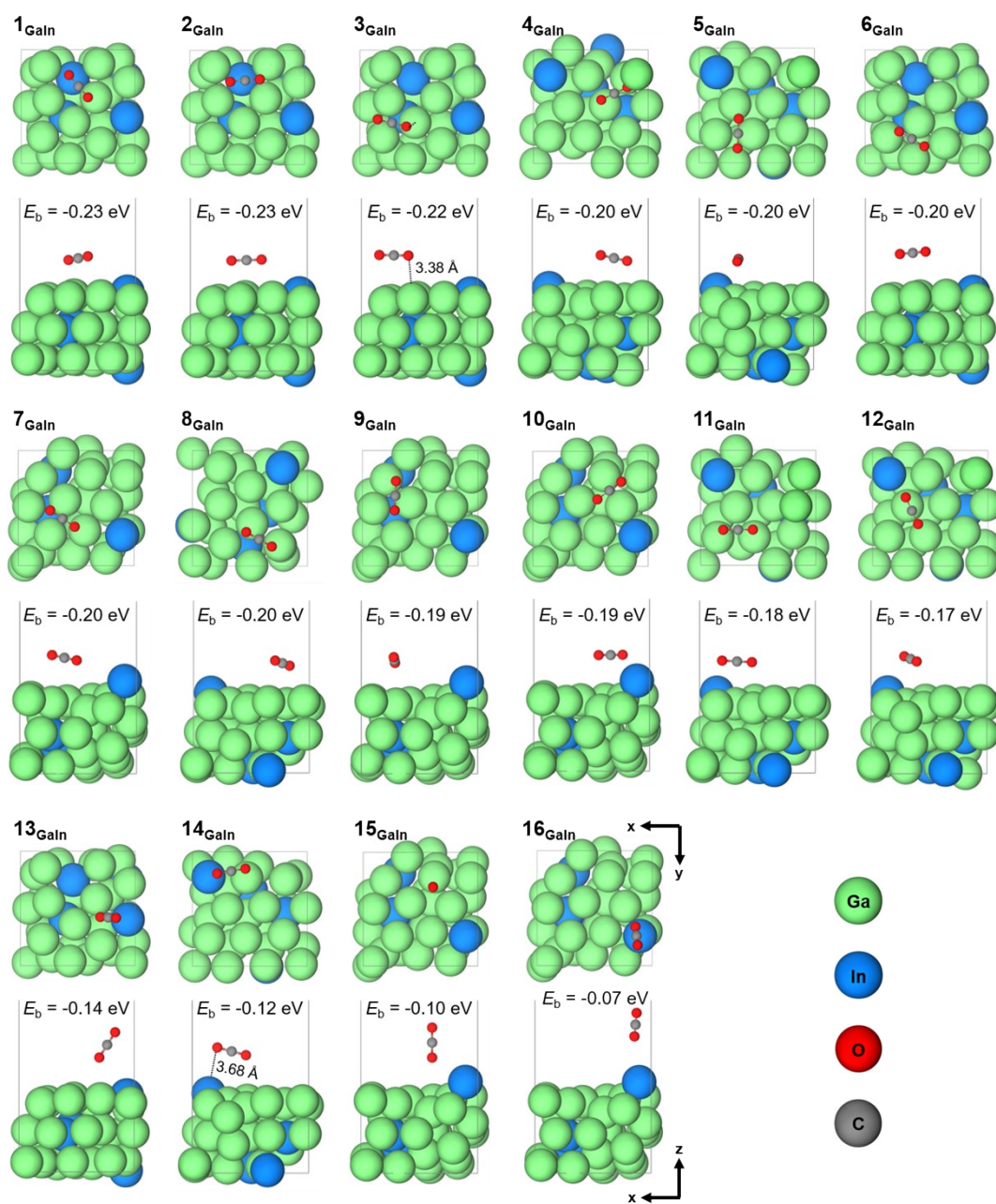


Fig. S14. The top and side views of the optimized CO_2/EGaIn structures (1 to 16_{GaIn}) and their binding energy (E_b) values.

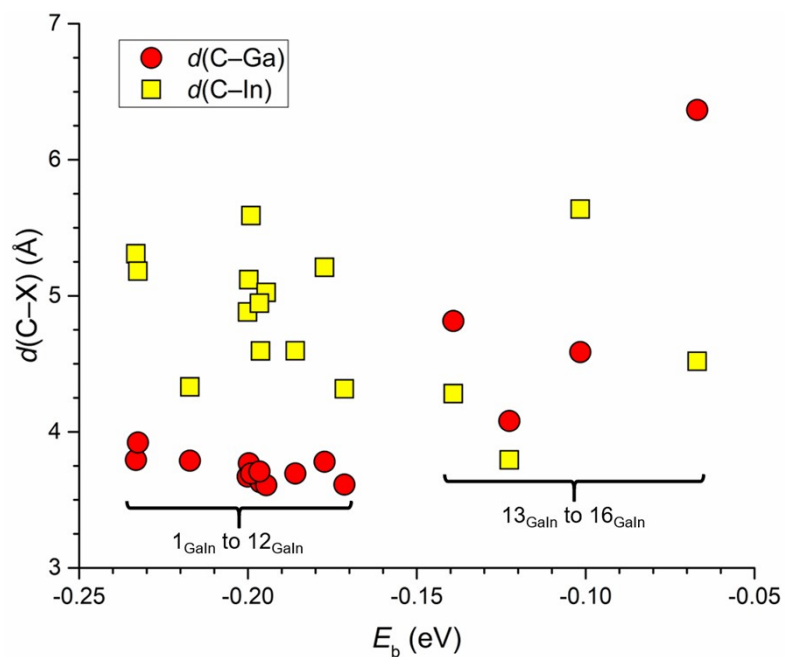


Fig. S15. The minimum distance between the C atom and Ga or In atom for the CO_2/EGaIn structures as a function of the binding energy (E_b) of each optimized structure.

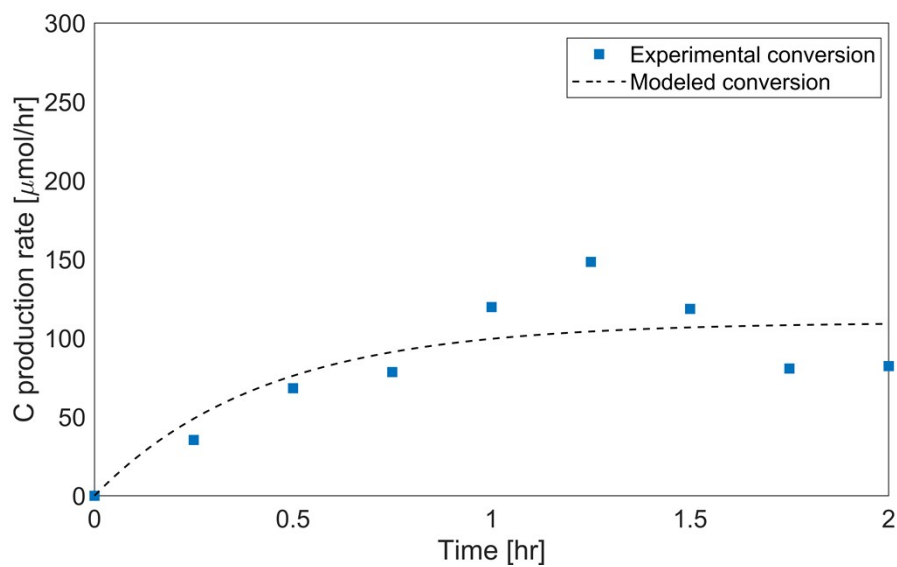


Fig. S16. Carbon production rate under continuous flow of 10% CO (balanced with Ar) at 200°C, showcasing the dissociation of CO using EGaIn.

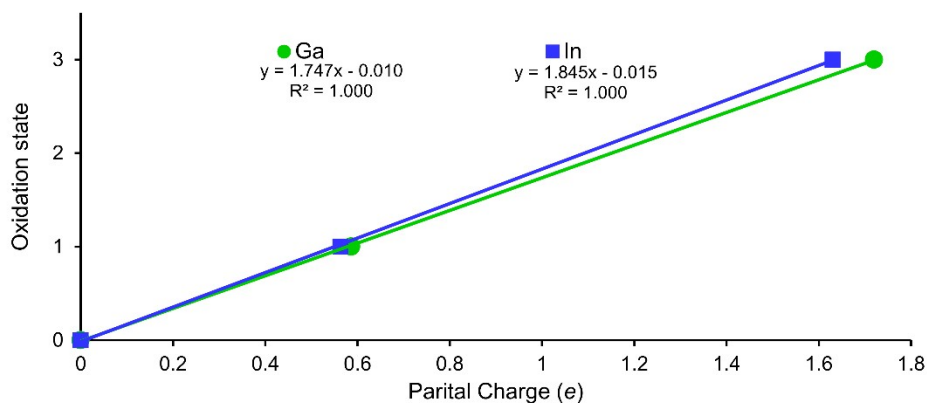


Fig. S17. The formal oxidation states of Ga in bulk Ga, Ga₂O₃, and the Ga₂O molecule, and In in bulk In, In₂O₃ and the In₂O molecule plotted against the corresponding partial charge of Ga or In.

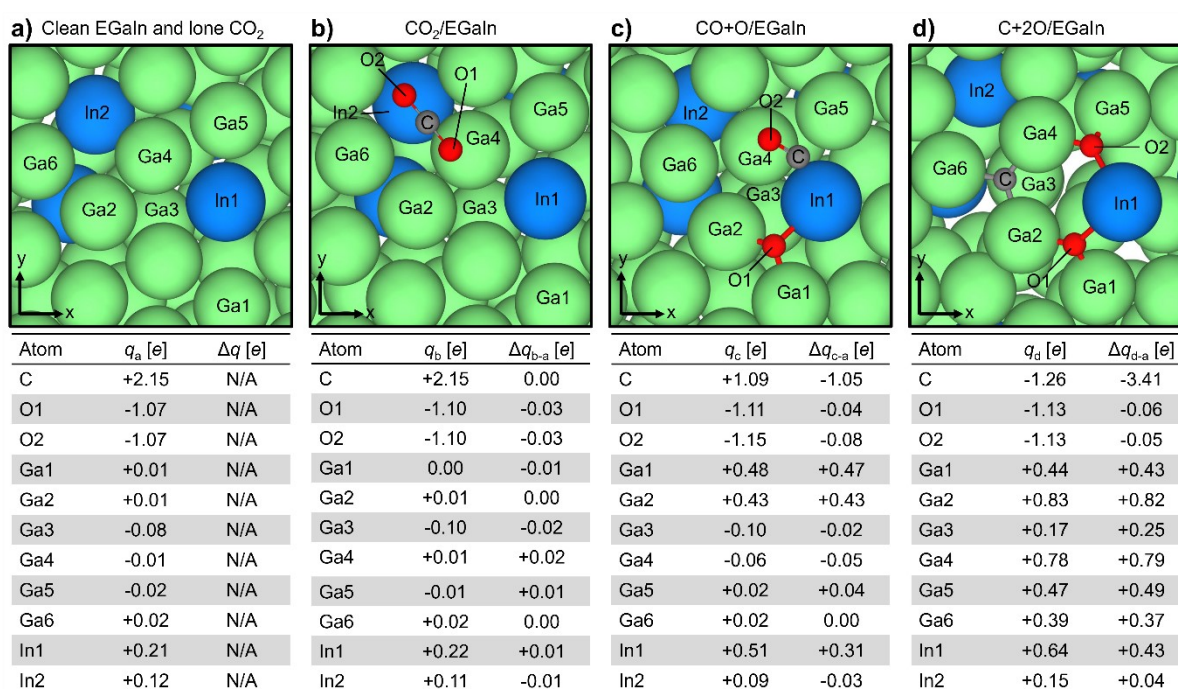


Fig. S18. The calculated partial charge (q) and the net change in charge (Δq) for selected atoms in the (a) clean EGaIn and isolated CO₂, (b) CO₂/EGaIn, (c) CO+O/EGaIn and (d) C+2O/EGaIn systems. The atoms of interest are labelled in a top-down view of each system.

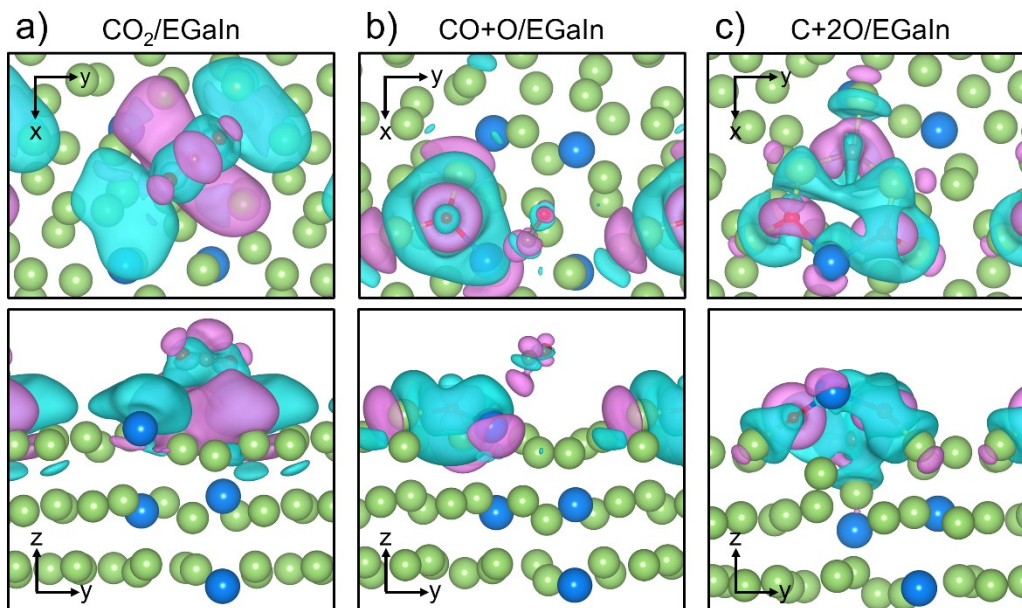


Fig. S19. Charge density difference plots of the a) CO_2/EGaIn , b) $\text{CO}+\text{O}/\text{EGaIn}$ and c) $\text{C}+2\text{O}/\text{EGaIn}$ systems with the top down and side views shown. Blue and magenta regions indicate charge depletion and accumulation, respectively.

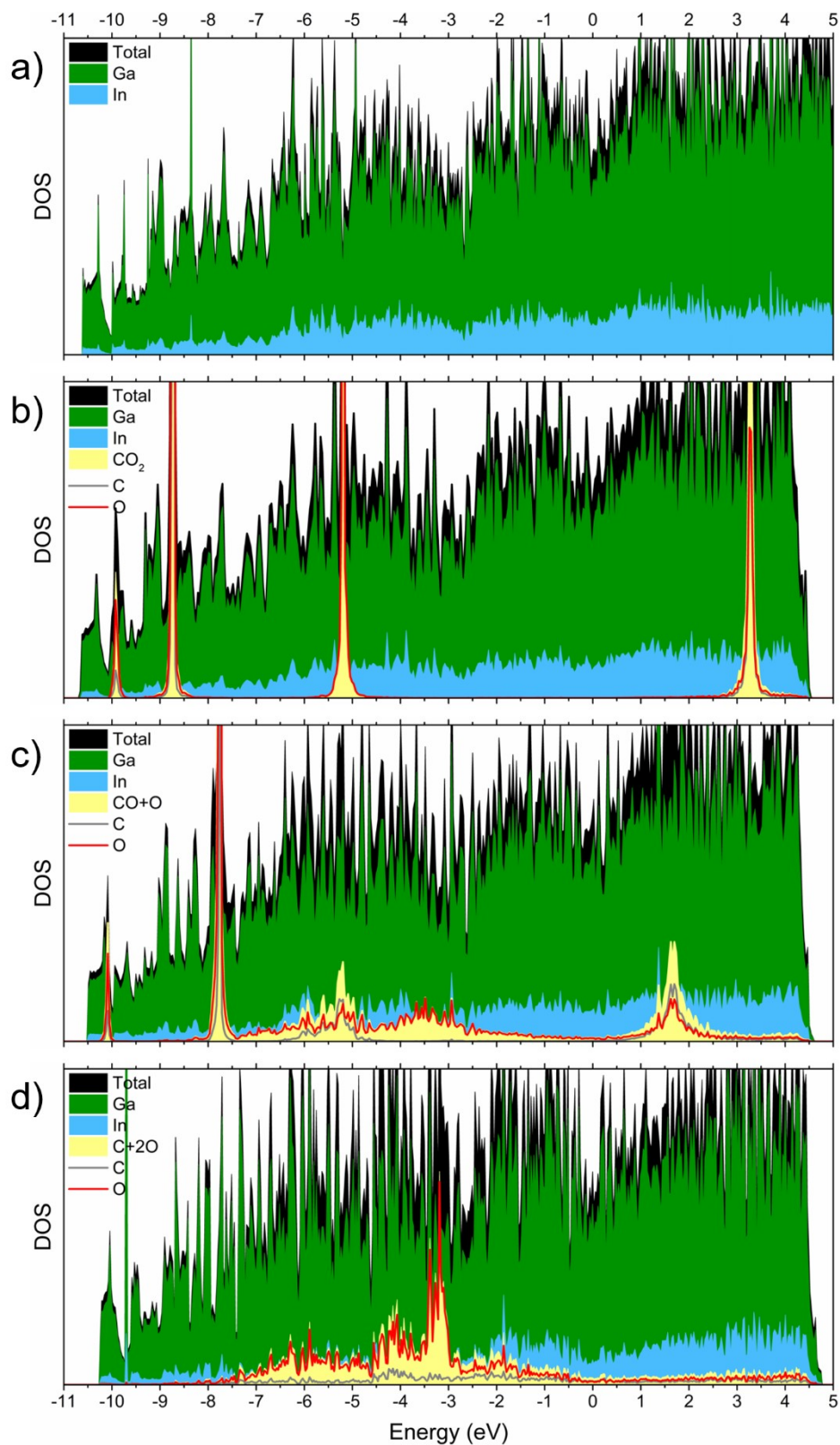


Fig. S20. The total and projected density of states (DOS) of the a) clean EGaIn, b) CO₂/EGaIn, c) CO+O/EGaIn and d) C+2O/EGaIn systems.

Table S1. The oxidation states of the Ga and In atoms from reference systems and the calibrated oxidation states of selected Ga and In atoms in the four different EGaIn systems noted.

System	Oxidation state									
	Ga	In	Ga1	Ga2	Ga3	Ga4	Ga5	Ga6	In1	In2
<i>Reference</i>										
Bulk Ga	0.00	–	–	–	–	–	–	–	–	–
Ga ₂ O molecule	+1.00	–	–	–	–	–	–	–	–	–
Bulk Ga ₂ O ₃	+3.00	–	–	–	–	–	–	–	–	–
Bulk In	–	0.00	–	–	–	–	–	–	–	–
In ₂ O molecule	–	+1.00	–	–	–	–	–	–	–	–
Bulk In ₂ O ₃	–	+3.00	–	–	–	–	–	–	–	–
<i>EGaIn</i>										
Clean EGaIn	–	–	+0.01	0.00	-0.15	-0.03	-0.04	+0.03	+0.37	+0.20
CO ₂ /EGaIn	–	–	-0.00	+0.01	-0.18	0.00	-0.02	+0.02	+0.38	+0.19
CO+O/EGaIn	–	–	+0.83	+0.75	-0.18	-0.12	+0.03	+0.03	+0.93	+0.15
C+2O/EGaIn	–	–	+0.76	+1.43	+0.29	+1.36	+0.82	+0.67	+1.16	+0.27

Table S2. Calculated partial charge (q) and net change in charge (Δq) for each of the atoms in the a) clean EGaIn and isolated CO₂ (q_a), b) CO₂/EGaIn (q_b), c) CO+O/EGaIn (q_c) and d) C+2O/EGaIn (q_d) systems.

Atom	q_a [e]	q_b [e]	Δq_{b-a} [e]	q_c [e]	Δq_{c-a} [e]	q_d [e]	Δq_{d-a} [e]
C	+2.15	+2.15	0.00	+1.09	-1.05	-1.26	-3.41
O1	-1.07	-1.10	-0.03	-1.11	-0.04	-1.13	-0.06
O2	-1.07	-1.10	-0.03	-1.15	-0.08	-1.13	-0.05
Ga1	+0.01	0.00	-0.01	+0.48	+0.47	+0.44	+0.43
Ga2	+0.01	+0.01	0.00	+0.43	+0.43	+0.83	+0.82
Ga3	-0.08	-0.10	-0.02	-0.10	-0.02	+0.17	+0.25
Ga4	-0.01	+0.01	+0.02	-0.06	-0.05	+0.78	+0.79
Ga5	-0.02	-0.01	+0.01	+0.02	+0.04	+0.47	+0.49
Ga6	+0.02	+0.02	0.00	+0.02	0.00	+0.39	+0.37
Ga7	-0.02	-0.02	+0.01	-0.03	0.00	+0.02	+0.04
Ga8	-0.07	-0.07	0.00	-0.09	-0.02	-0.12	-0.05
Ga9	0.00	-0.01	-0.01	-0.02	-0.02	-0.03	-0.04
Ga10	-0.12	-0.10	+0.01	-0.05	+0.07	-0.08	+0.04
Ga11	+0.01	+0.01	0.00	+0.05	+0.04	+0.01	0.00
Ga12	-0.04	-0.01	+0.03	-0.02	+0.03	-0.04	0.00
Ga13	+0.01	+0.00	-0.01	+0.03	+0.03	-0.06	-0.07
Ga14	-0.02	-0.03	-0.01	-0.08	-0.06	-0.01	+0.01
Ga15	-0.07	-0.08	-0.02	-0.10	-0.03	+0.04	+0.11
Ga16	-0.01	-0.03	-0.02	-0.03	-0.02	0.00	+0.01
Ga17	+0.03	+0.04	+0.01	-0.03	-0.05	-0.02	-0.05
Ga18	+0.05	+0.05	0.00	+0.07	+0.02	+0.01	-0.04
Ga19	-0.02	+0.01	+0.04	-0.02	0.00	-0.03	-0.01
Ga20	+0.06	+0.06	0.00	+0.03	-0.03	-0.02	-0.07
Ga21	-0.09	-0.05	+0.04	-0.07	+0.01	-0.15	-0.06
Ga22	+0.04	+0.01	-0.03	-0.02	-0.07	+0.07	+0.03
Ga23	-0.04	-0.05	-0.01	+0.02	+0.06	+0.03	+0.07
Ga24	0.00	+0.03	+0.03	+0.01	+0.01	-0.03	-0.03

Ga25	-0.10	-0.10	0.00	-0.05	+0.05	-0.05	+0.05
Ga26	+0.01	+0.02	+0.01	+0.02	+0.01	-0.01	-0.02
Ga27	-0.13	-0.12	+0.02	-0.07	+0.06	-0.05	+0.09
Ga28	-0.05	-0.11	-0.06	-0.11	-0.06	-0.07	-0.03
In1	+0.21	+0.22	+0.01	+0.51	+0.31	+0.64	+0.43
In2	+0.12	+0.11	-0.01	+0.09	-0.03	+0.15	+0.04
In3	+0.10	+0.10	0.00	+0.11	+0.01	+0.06	-0.04
In4	+0.22	+0.22	0.00	+0.22	0.00	+0.18	-0.04

Table S3. Space group of the unit cell, k-points used during the calculations, calculated average partial charge of Ga and In atoms in the 0, +1 or +3 oxidation states, and calculated lattice parameters of bulk Ga, Ga₂O₃, In, and In₂O₃, and the individual molecules Ga₂O and In₂O.

System	Space Group	k-points	Average partial charge (e)						Lattice Parameters (Å)		
			q(Ga ⁰)	q(Ga ¹⁺)	q(Ga ³⁺)	q(In ⁰)	q(In ¹⁺)	q(In ³⁺)	a	b	c
Bulk Ga	P1	19x19x19	0.00	–	–	–	–	–	4.54	7.71	4.56
Ga ₂ O*	P1	1x1x1	–	+0.59	–	–	–	–	20.00	20.00	20.00
Bulk Ga ₂ O ₃	C2/m	3x3x3	–	–	+1.72	–	–	–	12.43	3.08	5.89
Bulk In	I4/mmm	8x8x5	–	–	–	0.00	–	–	3.48	3.48	4.39
In ₂ O*	P1	1x1x1	–	–	–	–	+0.56	–	20.00	20.00	20.00
Bulk In ₂ O ₃	Ia $\bar{3}$	3x3x3	–	–	–	–	–	+1.63	8.92	8.92	8.92

*A cubic unit cell with fixed lattice parameters is used for calculations of the individual molecules Ga₂O and In₂O.

Supplementary Note 1: In-situ XPS measurements for CO₂ decomposition over EGaIn

The increase in the C – C carbon content and the absence of extra carbonaceous species indicate the deposition of pure carbon on the surface of EGaIn. Note that adventitious carbon is present on the surface of any sample and would as a result appear in any XPS spectrum. Since the appearance of adventitious carbon is an inevitable occurrence, the difference between the carbon peak before and during CO₂ decomposition is measured to determine the deposition of carbon as a product. Moreover, an inert gas transfer process that limits metal oxide formation was utilized prior to sample analysis to ensure that the gallium oxide content measured using XPS is an outcome of CO₂ splitting and is not generated by the native oxide.

Supplementary Note 2: Electrochemical reduction of Ga

The feasibility of the reduction process was validated by conducting the electrochemical reduction of gallium oxide in 1M H₂SO₄ solution on glassy carbon. The onset potential of the gallium deposition reaction was found at a significantly less negative potential (vs. Ag/AgCl) when compared with the onset of the hydrogen evolution reaction of a gallium-free reference solution (Fig. S11). This finding highlights the possibility of regenerating reacted gallium and closing the catalytic cycle. Furthermore, gallium reduction was also conducted in a two-electrode system which resembles a potential implemented process more closely. Here an onset potential of -1.57 V was measured, while a current density of 20 mA/cm² was obtained at -2.5 V. The use of an electrochemical approach to reduce the generated gallium oxide allows for the employment of established reactor designs that are compatible with renewable energy sources.

Supplementary Note 3: Interaction of CO₂ with Ga-In and pure Ga modeling

The DFT calculations show that CO₂ adsorbs on the Ga and In-doped Ga slab surfaces. CO₂ was found to bind more strongly to a surface Ga atom than to a surface In atom (Fig. S8) with the CO₂ aligned almost parallel to the surface. This is illustrated by the shorter distances (<4 Å) between C–Ga for structures 1–12_{GaIn} (Fig. S9). Conversely, weaker binding energies (for structures 13–16_{GaIn}) occurred when the CO₂ was adsorbed atop an In atom, typically resulting in a perpendicular orientation of the O–C–O plane with respect to the EGaIn slab. This results in the C–Ga distance increasing above 4 Å (Fig. S9) corresponding to a reduced interaction between the CO₂ and Ga atoms and weaker binding energies, even when the C–In distance is below <4 Å (for structure 14_{GaIn}).

Supplementary Note 4: Computational details

The Bader charge analysis method^{9, 10} was used to calculate the partial charge (*q*) of each individual atom of CO₂ and the EGaIn slab (Table S2). A high-density fast Fourier transform (FFT) grid (four times larger) was required to ensure the Bader charges were converged.

To deduce the oxidation state of Ga and In in the EGaIn slab, we compare the partial charges of key atoms with reference structures which have known oxidation states. The reference structures used include bulk Ga, In, Ga₂O₃ and In₂O₃, and a Ga₂O and In₂O molecule. The calculated partial charges of the Ga and In atoms in these systems (Table S3) are plotted against the formal oxidation states of Ga (0 in bulk Ga, +1 in the Ga₂O molecule and +3 in bulk Ga₂O₃) and In (0 in bulk In, +1 in the In₂O molecule, and +3 in bulk In₂O₃) (Fig. S17).

Linear relationships were determined between the formal oxidation states and partial charge values of the Ga (Equation S1) and In (Equation S2) atoms:

$$y = 1.747x - 0.010 \quad (\text{S1})$$

$$y = 1.845x - 0.015 \quad (\text{S2})$$

where x is the partial charge of Ga or In, and y is the corresponding oxidation state.

Using this linear relationship between the formal oxidation states and partial charge of Ga or In, the oxidation state of the Ga and In atoms of the EGaIn systems was estimated (Table S1).

The charge redistribution was determined by calculating the charge density difference where the charge density of the adsorbate (CO_2 , $\text{CO}+\text{O}$ or $\text{C}+2\text{O}$) and clean surface (EGaIn), were subtracted from the charge density of the reacted systems (CO_2/EGaIn , $\text{CO}+\text{O}/\text{EGaIn}$ or $\text{C}+2\text{O}/\text{EGaIn}$) (Fig. S19). Density of states (DOS) calculations were also performed for the EGaIn systems before and after the reaction with CO_2 (Fig. S20).

References

- 1 G. Kresse and J. Furthmüller, *Phys. Rev. B*, 1996, **54**, 11169-11186.
- 2 G. Kresse and J. Furthmüller, *Comput. Mater. Sci.*, 1996, **6**, 15-50.
- 3 G. Kresse and D. Joubert, *Phys. Rev. B*, 1999, **59**, 1758-1775.
- 4 G. Kresse and J. Hafner, *Phys. Rev. B*, 1993, **47**, 558-561.
- 5 J. P. Perdew, K. Burke and M. Ernzerhof, *Phys. Rev. Lett.*, 1996, **77**, 3865-3868.
- 6 P. E. Blöchl, *Phys. Rev. B Condens. Matter*, 1994, **50**, 17953-17979.
- 7 K. G. Steenbergen, D. Schebarchov and N. Gaston, *J. Chem. Phys.*, 2012, **137**, 144307.
- 8 S. Grimme, J. Antony, S. Ehrlich and H. Krieg, *J. Chem. Phys.*, 2010, **132**, 154104.
- 9 W. Tang, E. Sanville and G. Henkelman, *J. Phys.: Condens. Matter*, 2009, **21**, 084204.
- 10 G. Henkelman, A. Arnaldsson and H. Jónsson, *Comput. Mater. Sci.*, 2006, **36**, 354-360.